



# A preliminary study on the double cold wire gas metal arc welding process

P. D. C. Assunção<sup>1</sup> · R. A. Ribeiro<sup>2</sup> · P. M. G. P. Moreira<sup>3</sup> · E. M. Braga<sup>1</sup> · A. P. Gerlich<sup>2</sup>

Received: 5 October 2019 / Accepted: 27 January 2020 / Published online: 8 February 2020  
© Springer-Verlag London Ltd., part of Springer Nature 2020

## Abstract

The increasing demands in productivity and reliability in welding have led to the development of newer welding processes. These processes frequently have superior deposition rates; however, they might lead to a wider heat-affected zone (HAZ) which might impair their mechanical properties. Here, a promising process termed the double cold wire gas metal arc welding (DCW-GMAW) is evaluated, offering higher deposition rates via feeding two cold wires into the weld pool to improve productivity. In contrast to similar processes, the HAZ of DCW-GMAW welds are smaller than gas metal arc welding (GMAW) welds. This work reports a preliminary assessment of the feasibility of the process in terms of electrical arc characteristics and stability. High-speed video acquisition was used to analyze the metal transfer across the arc. Finally, standard metallographic techniques and Vickers hardness were used to assess the weld cross sections and microstructures. The results demonstrate the feasibility of DCW-GMAW based on the process stability at different cold wire feed rates while also offering high deposition (high productivity) of weld deposits with desirable hardness due to increased acicular ferrite content.

**Keywords** Standard GMAW · DCW-GMAW · Metal transfer · Cross sections · Macro- and micrographs

## 1 Introduction

The melting and deposition rate of welding consumables (kg/h) determines the productivity in welding. This is an issue for many applications, for instance shipbuilding where high-energy processes such as submerged arc welding (SAW) is used [1]. Yet for heavy-duty welding applications, high productivity often comes at the expense of deterioration of the heat-affected zone properties by excessive heat transferred to the workpiece which impair the mechanical properties of the joints. Ideally, a process to be considered in heavy-duty

welding should both be productive and avoid deterioration of the heat-affected zone (HAZ) which can occur with excessive heat input [2].

Recently, SAW modifications through improved flux composition with increased fraction of TiO<sub>2</sub> [3] reported increased fractions of acicular ferrite (AF) through increase of inclusions in the weld metal, which improved mechanical properties, for instance the Charpy impact properties. The reason behind this improvement in acicular ferrite content is that this microphase nucleates on inclusions as reported by Babu [4]. Further studies, employing the cold wire in SAW, showed that the fatigue crack threshold increases in the weld metal fabricated [5]. However, an issue in SAW is that the process is only applicable in flat position which compromises its application in welds out of flat position.

Tandem gas metal arc welding (T-GMAW) has been used to replace SAW. Larkin et al. [6] reported that T-GMAW has superior versatility in conjunction with higher travel speed, decreasing the HAZ area while diminishing the post welding distortion. A drawback for T-GMAW is that even when using two torches, the deposition is normally still below that of the conventional SAW. Other techniques, such as hybrid laser, have been used in specific shipbuilding applications. For instance, Turichin et al. [7] reported the welding of steel panels

✉ R. A. Ribeiro  
rdearauj@uwaterloo.ca

<sup>1</sup> Metallic Materials Characterization Laboratory (LCAM), Federal University of Pará (UFPA), Rua Augusto Corrêa, 1 - Guamá, Belém, PA 66075-110, Brazil

<sup>2</sup> Center for Advanced Materials Joining (CAMJ), University of Waterloo, 200 University Avenue West., Waterloo., Ontario, N2L 3G1, Canada

<sup>3</sup> INEGI, Institute of Science and Innovation in Mechanical and Industrial Engineering, R. Dr. Roberto Frias 400, 4200-465 Porto, Portugal

up to 45 mm thick used in shipbuilding applications. Hybrid laser welding also has difficulty in matching the deposition of SAW; however, the heat input and HAZ deterioration are much lower. Recent studies, for instance by Nastrom et al. [8], operationalized the welding of a near-vertical narrow gap joint reducing re-heating time and robustness. These results could easily be applied in ship construction, for example, although the cost associated with this arc-laser hybrid process is still prohibitive.

A recent modification of the standard GMAW that was developed specifically for shipbuilding applications is called the cold wire gas metal arc welding (CW-GMAW). This process involves feeding non-energized wire into the welding pool to be melted by the surplus heat that would otherwise be lost. Ribeiro et al. [9] studied this process and reported a decrease in dilution while increasing the melting wire rate. Further afield, Costa Assunção et al. [10] reported the feasibility to utilize CW-GMAW for narrow gap welding (NGW), considering the advantages in avoiding sidewall erosion. Further information regarding NGW wide applicability and advantages in reducing distortion, residual stresses, while increasing productivity was reported by Malin [11, 12].

Moreover, Cabral et al. [13], employing this process to weld marine panels, reported improved results in angular distortion when compared with standard GMAW. Marques et al. [14] reported that joints manufactured using CW-GMAW present superior fatigue life compared to GMAW joints due to a favorable microstructure. Subsequently, Costa et al. [15] measured the residual stresses in CW-GMAW welds in comparison to standard GMAW using two different methods. It was concluded that CW-GMAW presents lower residual stresses than standard GMAW.

In order to further increase the productivity of CW-GMAW, Braga and Costa Assunção [16] proposed the double cold wire gas metal arc welding (DCW-GMAW) process in 2013. This work reports a feasibility study of DCW-GMAW with a possible use in heavy applications such as in shipbuilding and infrastructure. This variant of GMAW consists of two non-energized wires fed into the welding pool to increase deposition without an increase in transferred heat. The feasibility is assessed based on arc stability, metal transfer dynamics, bead aspect, and microstructure. To the authors' best knowledge, this is the first time these issues are reported to the welding community.

## 2 Experimental methods and set-up

Bead on plate and narrow groove welds were performed using a R500 Lincoln robotic welding power source operating in constant voltage (CV) mode. The set-up for the positioning of the cold wires regarding the electrode wire is shown in Fig. 1. The welding parameters used were found

experimentally through trial and error in a prior study. The parameters used for the weld fabrication in GMAW and DCW-GMAW can be seen in Table 1. One can see that the cold wire feed rate was varied to assess its influence on the process and microstructure. The cold wire feed values refer to the quantity in mass percentage fed in each cold wire, i.e., the mass feed rate of the electrode in kilogram per second, and percentage fractions of it were used to determine the cold wire rates. The contact tip to workpiece (CTWD) distance was equal to 17 mm.

The average instantaneous voltage ( $\bar{U}_{\text{avg}}$ ), average instantaneous current ( $\bar{I}_{\text{avg}}$ ), and the average instantaneous power ( $\bar{P}_{\text{avg}}$ ) were calculated according to the recommendation of Joseph et al. [17] through:

$$\bar{U}_{\text{avg}} = \frac{1}{n} \sum_{i=1}^n U_i \quad (1)$$

$$\bar{I}_{\text{avg}} = \frac{1}{n} \sum_{i=1}^n I_i \quad (2)$$

$$\bar{P}_{\text{avg}} = \frac{1}{n} \sum_{i=1}^n U_i \cdot I_i \quad (3)$$

where  $U_i$  and  $I_i$  are the instantaneous values of voltage and current, respectively. The nominal energy (kJ/mm) was calculated by dividing the instantaneous average power by the travel speed in millimeters per second. In order to assess the arc stability of the voltage signal, the coefficient of variation (COV) of voltage was calculated:

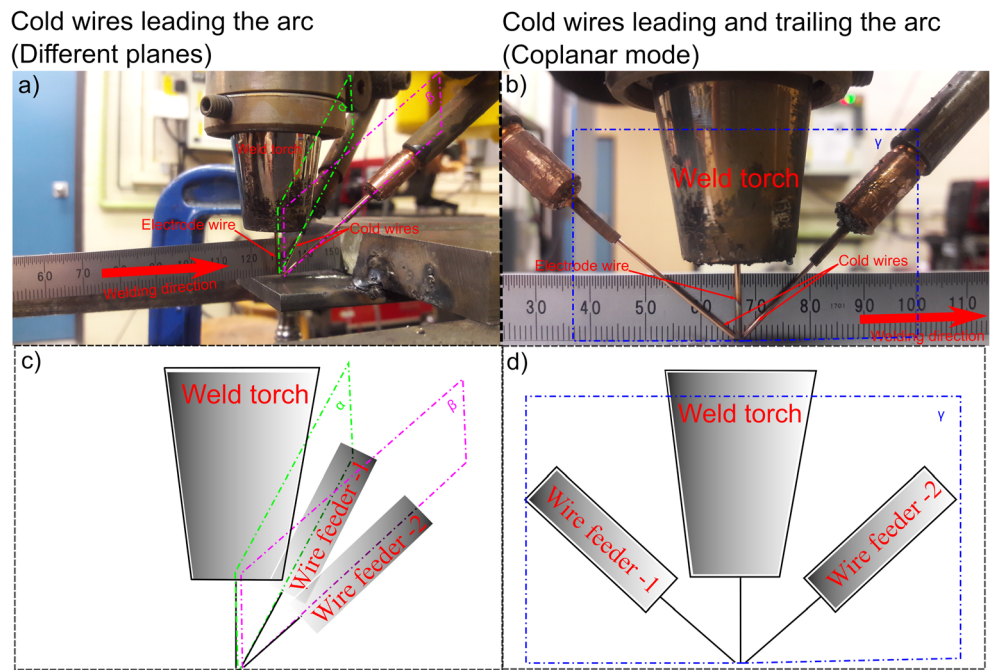
$$\text{COV}_{\text{voltage}} = \frac{\sigma_{\text{voltage}}}{\bar{U}_{\text{avg}}} \quad (4)$$

where  $\sigma_{\text{voltage}}$  is the voltage standard deviation and  $\bar{U}_{\text{avg}}$  is the instantaneous average voltage. In general, a high COV indicates low stability, and contrarily, a low COV indicates high stability.

The bead on plate welds were deposited over hot rolled AISI 1020 plain carbon steel flat bars. The shielding gas used was Ar-15%  $\text{CO}_2$  at a flow rate of 40  $\text{ft}^3/\text{h}$ . The nominal chemical compositions of the steel and ER70S-6 wires used for the bead on plate welds are provided in Table 2 according to references [18, 19], respectively.

In parallel, current and voltage were acquired with synchronized high-speed imaging, using a data acquisition (DAQ) system (which consisted of a National Instruments DAQ system, a Hall sensor to measure current from the welding lead, and a resistive voltage divider to measure torch voltage), to investigate the arc dynamics. The videos were performed using a FastCam mini UX50 at 5000 fps with an aperture of f/22, shutter speed of 25 ms, and a band pass filter of 910 nm to limit the amount of arc light reaching the camera sensor. The electrical signals were acquired at 10 kHz for 2 s. After welding, the specimens were cross sectioned and

**Fig. 1** Set-up for cold wire position: **a, c** Leading the arc **b, d** Leading and trailing the arc



subjected to standard metallographic procedures. The cross sections were etched with 5% Nital. The geometric features of the bead were measured using an image processing software. The microstructures were observed through optical microscopy. The microstructures were analyzed according to the International Institute of Welding (IIW) guidelines for optical microscopy nomenclature of ferritic steels [20].

Moreover, Vickers hardness was mapped on the weld beads using a load of 500 gf and dwell time of 10 s. In total, 20 columns × 22 rows were performed in order to study the weld metal, HAZ, and base metal. The location where the indentations were performed is given in the figure where the hardness results are presented.

### 3 Results

#### 3.1 Electrical data summary

Table 3 shows the average values of current, voltage, and power along with the energy density for each process. It was found that the average current increases as the power source is

operating in constant voltage and an increase in mass rate caused by the cold wires causes the current to increase in order to accommodate the extra material, leading to an increase in energy density, which is consistent with our prior work [9].

The average instantaneous voltage also indicates that the arc is more stable as the cold wire feed rates increase, given that it is closer to the voltage set point of 28 V, even when the cold wire feed rates increase, indicating that the addition of cold wire improves the voltage response of the welding power.

#### 3.2 Oscillograms and arc stability

The collected measurements for current and voltage have been represented as oscillograms for the entire sampling time of 2000 ms in order to assess the arc stability of the welding conditions presented in this work. Basically, the arc stability was assessed based on the COV for voltage since this welding parameter is controlled in constant voltage mode. A lower COV indicates a more stable welding regime since this will be correlated with a more consistent arc length which will facilitate a more consistent transfer which accounts for the higher stability observed.

**Table 1** Experimental matrix, with the parameters set in the welding source and variation in cold wire feeding

Process	Cold wire mass fraction percentage (%) <sup>a</sup>	Wire feed speed (in./min)	Voltage (V)	Travel speed (in./min)
Standard GMAW	0	310	28	25
DCW-GMAW	20	310	28	25
	40	310	28	25
	60	310	28	25

<sup>a</sup> This represents the mass fraction fed through each injector

**Table 2** Nominal chemical composition of the welding wires and the base metal

Material	C	Mn	P	S	Ti	Mo	Ni	Cr	Fe
ER70S-6	0.15	1.85	–	0.035	–	–	–	–	Bal.
AISI 1020	0.18	0.30	–	Max. 0.005	–	–	–	–	Bal.

One can see that the introduction of the cold wires leads to the stabilization of the voltage set-point. In particular, in constant voltage, voltage is closely correlated to arc length. Xiang et al. [21] reported that the introduction of cold wire leads to stabilization of emitting cathode spots. This seems to be consistent with the pinning of the arc to the (Fig. 2), cold wire observed by Costa Assunção et al. [10].

### 3.3 Cyclogrammes

In order to have a thorough understanding of the dynamic behavior of the electric arc, Fig. 3 presents the cyclogrammes for all the welding conditions. Cyclogrammes provide a comparison of the current versus voltage history in order to indicate overall arc stability and reveal trends in the arc behavior such as short circuits. The area of the cyclogramme can be correlated to arc stability, and so, a larger area implies lower stability and, contrary-wise, a smaller one implies higher stability. Further details on cyclogrammes can be found in the work by Jorge et al. [22].

It can be seen that the cyclogramme obtained on standard GMAW (Fig. 3a) presents some points towards the higher voltage and lower current region (superior left corner). This behavior indicates some arc instabilities related to a longer arc length. Moreover, one can see that as the cold wire is fed into the arc-weld pool, the stability of the process improves overall (Fig. 3b–e). This seems consistent with the results reported by Xiang et al. [21] who reported that the addition of a cold wire in twin GMAW improves stability due to stabilization of the wandering of the electron-emitting cathode spots. Also, the stability is slightly improved when the two cold wires are fed in coplanar mode (Fig. 3e) compared to when they are fed at the leading edge of the arc, refer to Fig. 3b.

**Table 3** Average values of current, voltage, and power sampled during welding

Process	Average instantaneous current (A)	Average instantaneous voltage (V)	Average instantaneous power (W)	Energy (kJ/mm)
GMAW	265	27.79	7363	0.69
DCW-20%	260	27.84	7501	0.71
DCW-40%	278	27.84	7755	0.73
DCW-60%	277	27.82	7705	0.73
DCW-60% coplanar	281	27.86	7830	0.74

### 3.4 High-speed videos and metal transfer mechanism

Figure 4 shows the high-speed images synchronized with electrical signals for the standard GMAW condition. The transfer mode achieved presents globular behavior, as the droplet diameter is not smaller than the wire electrode diameter. The voltage and current present some scatter around 28 V (voltage set-point) and 265 A, respectively.

It can be verified in Fig. 5a that current variation in DCW-GMAW-40% is still similar to standard GMAW which is consistent with what is shown in Table 3. The droplet detachment period is about 0.4 ms, which is consistent with a slight increase in electromagnetic detachment which is proportional to the current increase to melt the extra wire fraction.

Likewise, the droplet detachment period in CW-GMAW-40% (Fig. 5b) is smaller than in CW-GMAW-20%, around 0.2 ms due to the fact that current increased again to vary around 285 A. Moreover, one can see that the arc becomes slightly attached to the two cold wires at this feed rate. Basically, the attachment is caused by the shortest current path flow from the arc to the wires. In addition, as the arc is pinned to the two cold wires, the weld pool penetration should decrease. The effect of the process parameters on the geometry of the beads will be discussed later in Sect. 3.5.

Figure 6a shows the CW-GMAW-60% when the cold wires are fed into the leading edge of the arc (tangent planes) and compared to when the cold wires are fed in a coplanar position in Fig. 6b. For the feed rate of CW-GMAW-60%, the arc is completely pinned to the cold wires. Contrary to expectations, when applying a feed rate of CW-GMAW-60%, the current does not increase and is kept in the expected limit of variation. One can find that with CW-GMAW-60%, it appears to have reached a stability limit as suggested by the respective cyclogramme (Fig. 3d). However, feeding the cold wires at the coplanar orientation seems to overcome this stability issue as can be seen in Fig. 3d.

It can be denoted in Fig. 6b that the arc is pinned to the cold wires fed in the same plane (coplanar). The weld pool is protected from the arc by the two wires, which will limit the penetration in this set-up. The current varies around 280 A, in average, as shown in Table 3, and it can be seen in Fig. 6 that the local current level for that time interval is similar to that of the standard GMAW.

Feeding the two cold wires coplanarly decreases the current and the HAZ which is beneficial for many applications, such as hard-facing. Another application could be narrow gap welding since this double arc pinning might avoid the sidewall erosion of the arc.

### 3.5 Bead characteristics

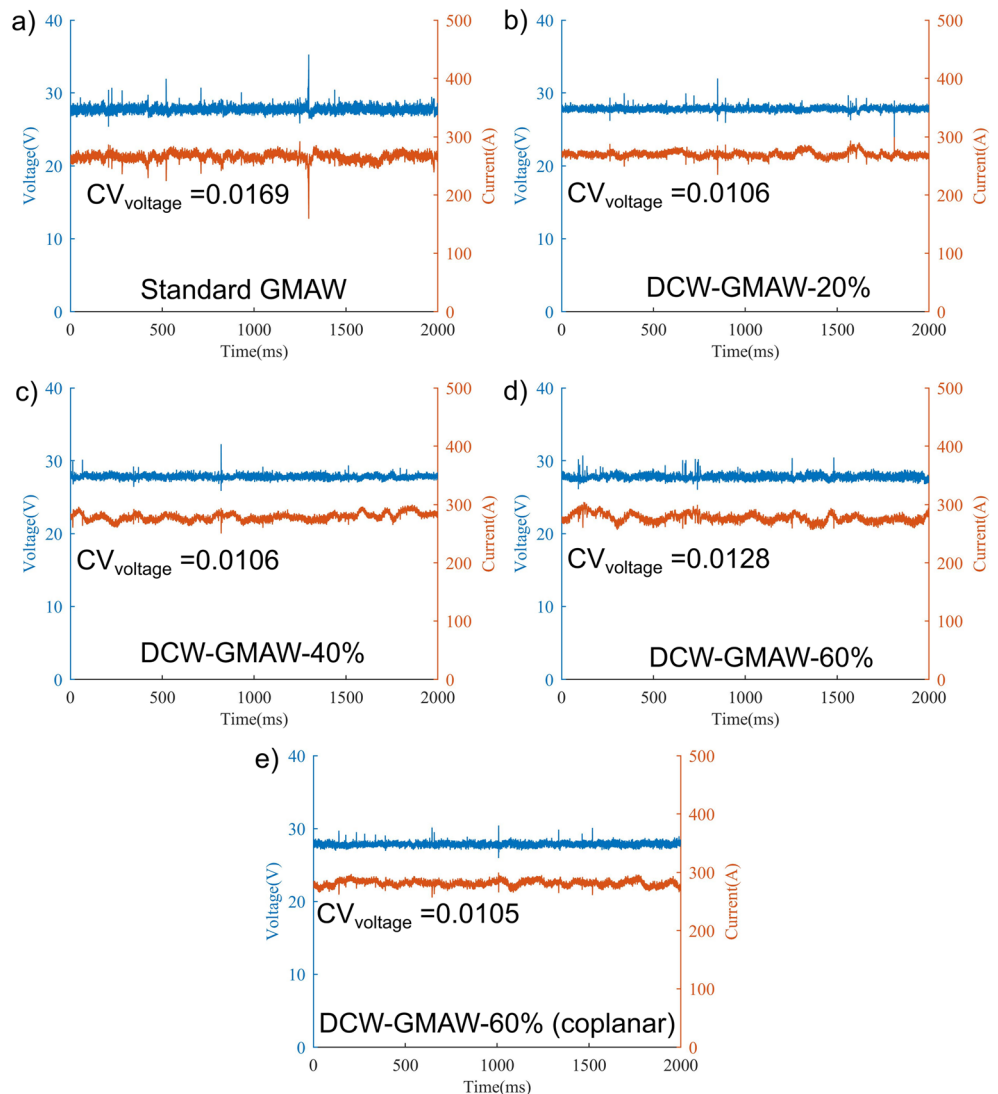
Figure 7 shows the features of the beads in all the welds. It can be observed that no superficial defects can be found in all conditions. Moreover, the level of spatter, as supported by the spatter adjacent to the weld beads, was low for all conditions, even at DCW-GMAW-60%. This indicates the stability and robustness of the process. The width of the weld pool seems to decrease as cold wire is fed, which might affect the Peclet ( $Pe$ ) number; this will be further evaluated in Sect. 4.

Also DCW-GMAW-60% (Fig. 7d) promotes an asymmetric weld pool. This phenomenon seems to be linked to the introduction of a higher cold wire rate into one part of the weld pool. When the same cold wire feed rate is introduced into two regions of the weld pool, as in the coplanar mode, for DCW-GMAW-60% (Fig. 7e), the weld pool symmetry is similar to the one obtained in standard GMAW (Fig. 7a).

### 3.6 Macrographs, penetration, and dilution

Figure 8 shows the macrographs for the conditions studied in this work. One can see that as the cold wire feed increases, the penetration decreases, with a consequent increase in the bead height. All the beads with feed rates up to DCW-GMAW-40% have a finger-like penetration, which is typical of axial metal transfer across the electric arc. This kind of penetration is suppressed by the cold wire feed since the cold wires shield

**Fig. 2** Oscillograms and voltage coefficient of variations: **a** Standard GMAW, **b** DCW-GMAW-20%, **c** DCW-GMAW-40%, **d** DCW-GMAW-60%, **e** DCW-GMAW-60%-coplanar



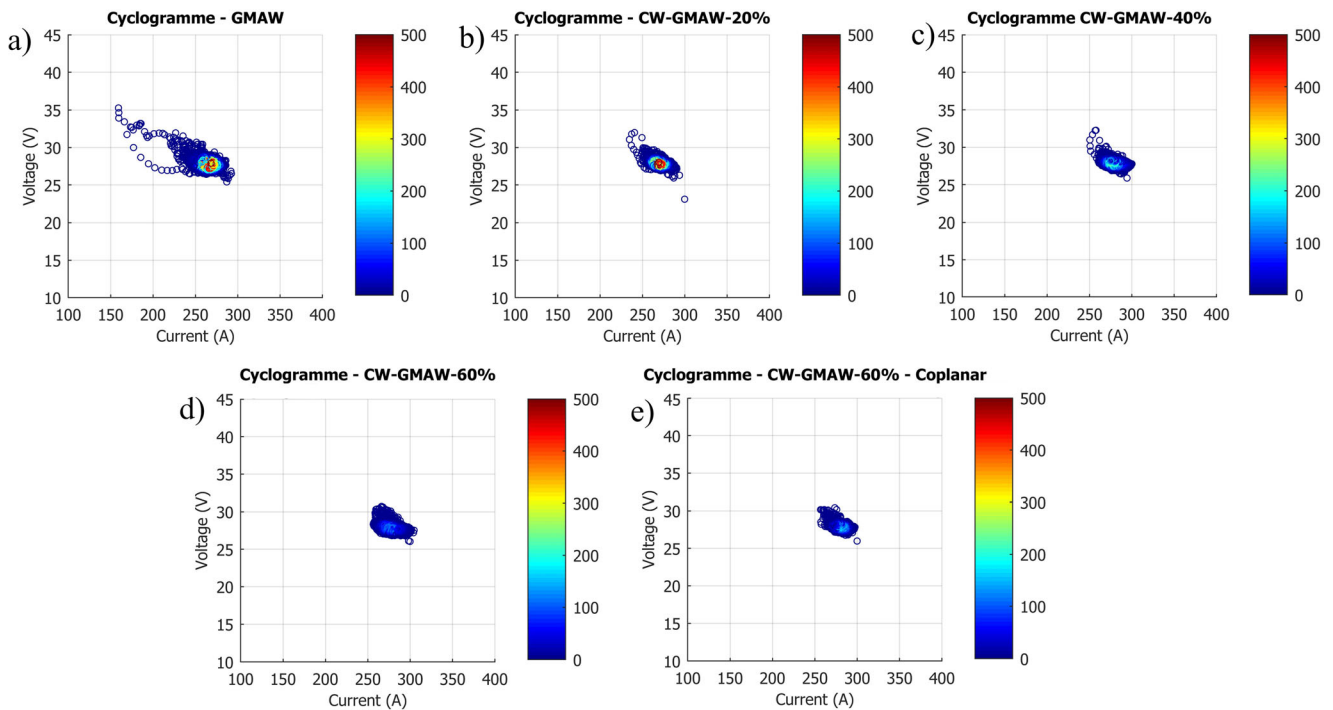


**Fig. 3** Cyclogrammes for welding conditions: **a** Standard GMAW. **b** DCW-GMAW-20%. **c** DCW-GMAW-40%. **d** DCW-GMAW-60%. **e** DCW-GMAW-60%-coplanar. Color bar indicates density of data points

the weld pool and avoid axial excavation by the impinging droplet.

However, when the two cold wires are fed in a coplanar alignment, this kind of penetration reappears. Most likely, when the cold wires are coplanar, not all droplets are shielded and some still excavate the weld pool.

The penetration and dilution for different cold wire feed rates are shown in Fig. 9. The penetration, as mentioned, decreases substantially with the increase of cold wire feed (Fig. 9a). This implies a desirable characteristic for applications such as hard-facing of wear-resistant alloys. However, joining applications cannot be disregarded since the reduction

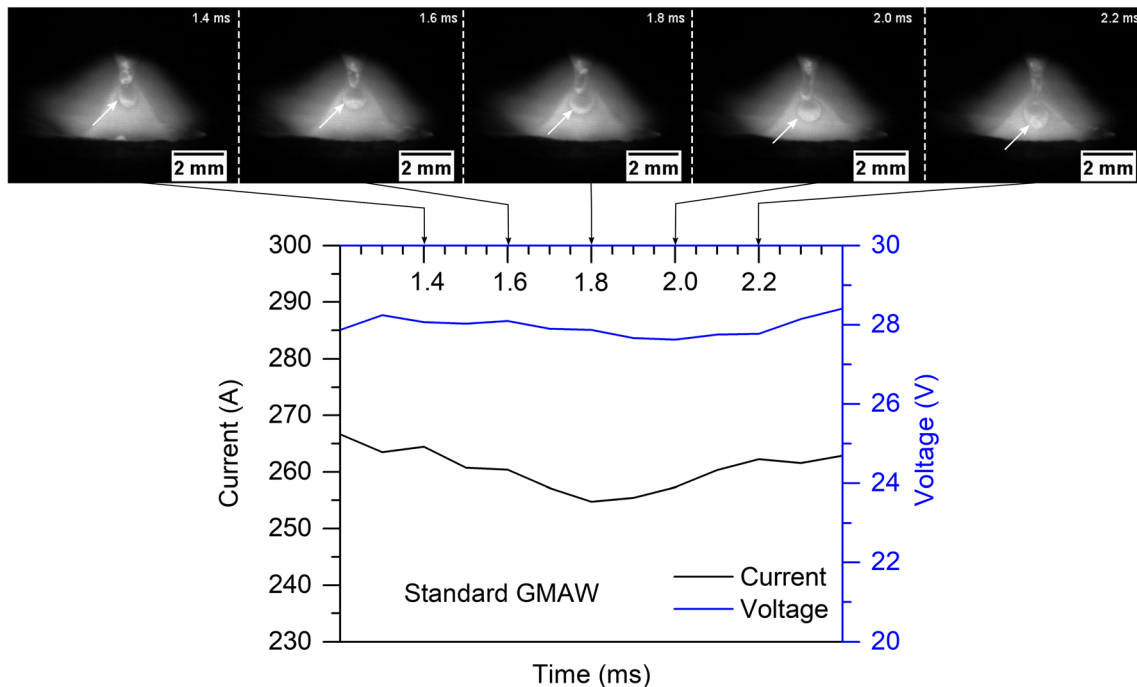


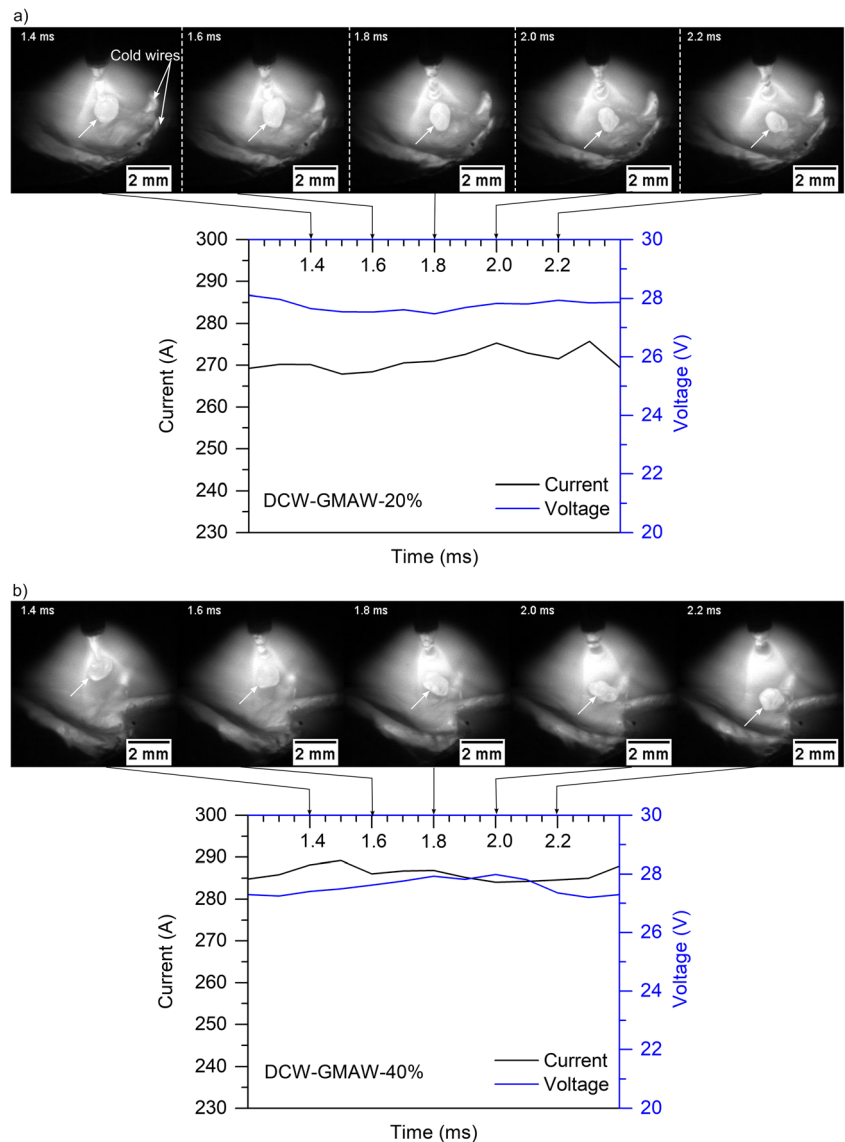
**Fig. 4** High-speed images of the arc synchronized with electrical signals: standard GMAW. The white arrow indicates the droplet detachment

in dilution might be interesting for some applications where groove dilution is an issue.

Also, the melting efficiency of the DCW-GMA welds is likely higher since an increase in the area due to added filler metal in the bead increases the overall melting efficiency. As noticed by Ribeiro et al. [23] for one cold wire, the DCW-GMAW also has an inverse relation between melting efficiency and dilution (Fig. 9b).

The trend in Fig. 9a, b shows that when the cold wires are fed in a coplanar way, there is a slight increase in penetration and dilution, which is consistent with the fact that not all the droplets are shielded by the cold wire and thus may axially excavate the weld pool (in spray transfer mode), increasing penetration and dilution, respectively.

**Fig. 5** High-speed images of the arc synchronized with electrical signals: **a** DCW-GMAW-20%, **b** DCW-GMAW-40%. The white arrow indicates the droplet detachment



### 3.7 Micrographs

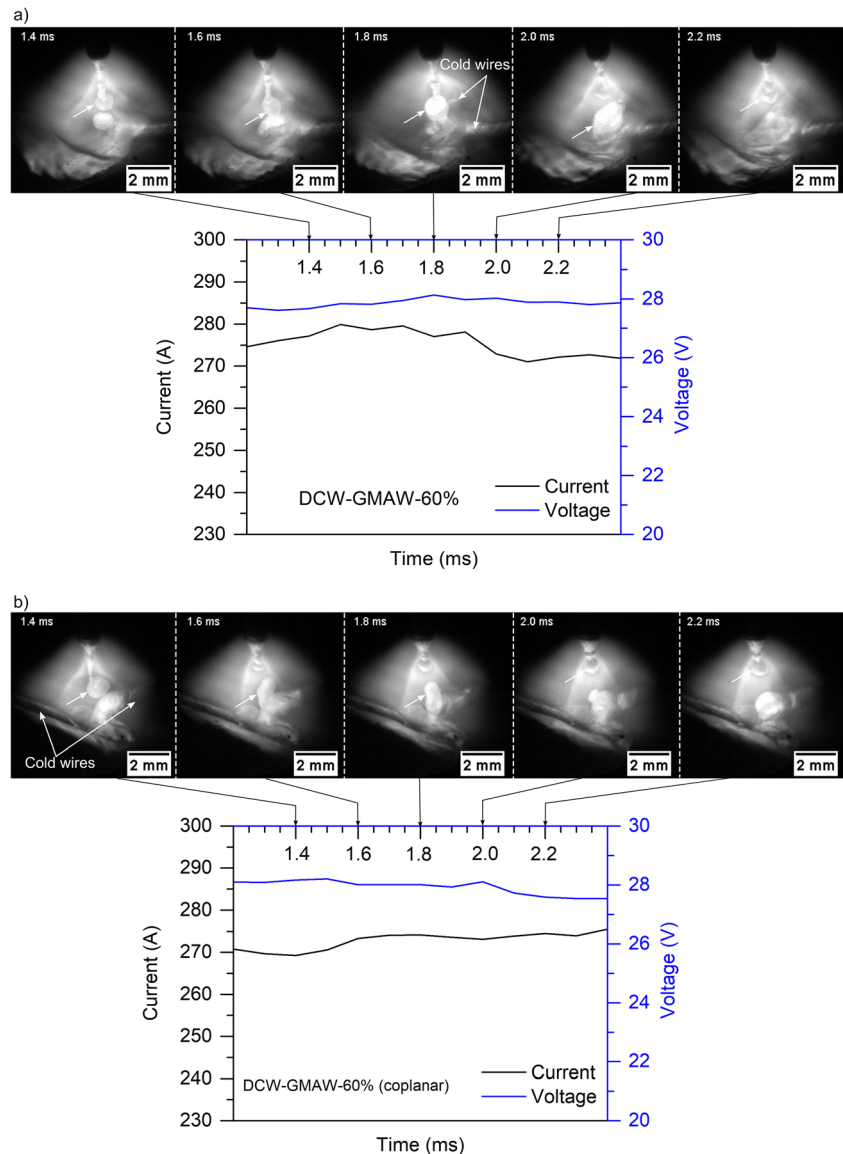
Figure 10 shows the micrographs of the beads shown in Fig. 8. The images were taken at the center of the beads. The standard GMAW specimen shows that the microstructure consists of primary ferrite in grain boundaries (PF(G)), ferrite with aligned second phase (FS(A)), ferrite with non-aligned second phase (FS(NA)), and acicular ferrite (AF).

The increase of the cold wire feed has negligible influence on the content of AF at the center of the bead. This likely means that the cooling rate at the center of the bead is the same in DCW-GMAW compared to GMAW. This likely implies that the cooling rate experienced by the weld metal differs from the cooling rate in DCW, which explains the difference in AF content. However, once the cold wires are

injected in coplanar mode, the weld metal presents again FS(A) which has been suppressed in DCW-20% to DCW-60%.

Another factor which can play a role on the fraction of AF microconstituents is the amount of inclusions that are formed in the weld metal which are active in AF nucleation. Again, one could assume that as two cold wires are fed, the number of oxides (inclusions) inside the welding pool would be higher which would increase the possibility of nucleation of AF given a favorable cooling rate. However, this was not observed during the characterization step of the welds. Moreover, the presence of AF is beneficial for strength and toughness of the weld metal given the interlocking morphology of this microstructure according to Abson and Byun et al. [24, 25].

**Fig. 6** High-speed images of the arc synchronized with electrical signals: **a** DCW-GMAW-60%, **b** DCW-GMAW-60%-coplanar. The white arrow indicates the droplet detachment



### 3.8 Vickers hardness

Figure 11 shows the Vickers hardness results for the DCW welds. The hardness results are consistent with the microstructures observed. It can be noted that the hardness of the DCW-20%, DCW-40%, and DCW-60% specimens is higher than that of the standard GMAW specimen. The exception being DCW-60% in the coplanar configuration in which the hardness of this specimen is lower than the other DCW specimen and similar to the standard GMAW.

The hardness results indicate that there are changes regarding the cooling rates of the DCW-GMAW specimens when compared to the GMAW specimen. The DCW-GMAW specimens (DCW-20%, DCW-40%, and DCW-60%) present higher cooling rates than the standard GMAW which account for the higher measured hardness. Again, the exception is



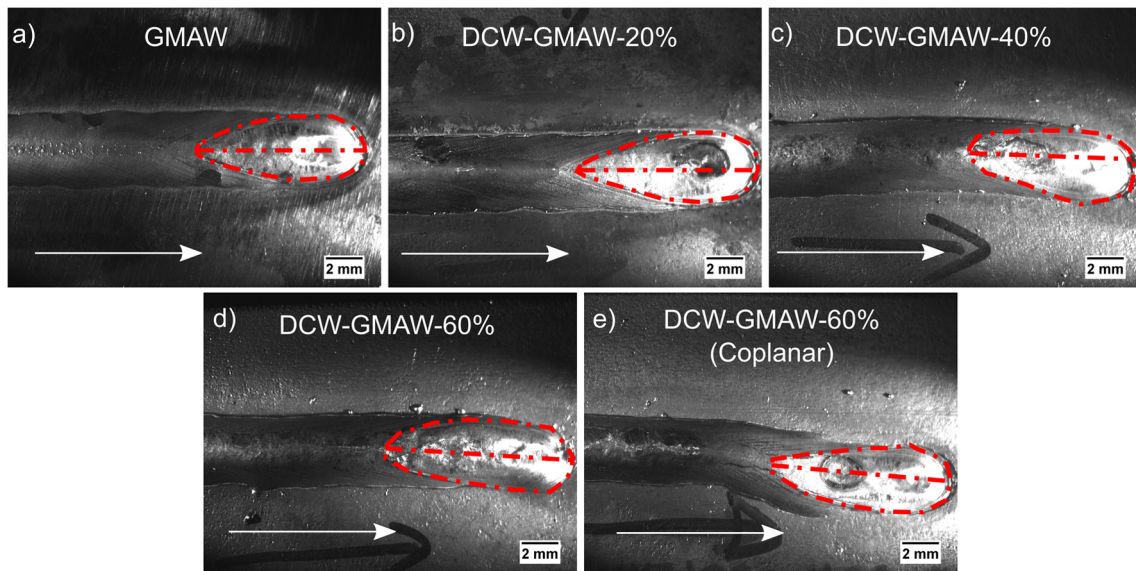


**Fig. 7** Weld bead characteristics: **a** standard GMAW, **b** DCW-GMAW-20%, **c** DCW-GMAW-40%, **d** DCW-GMAW-60%, **e** DCW-GMAW-60%-coplanar. The white arrow indicates the welding direction

DCW-GMAW-60%-coplanar which presents similar hardness, and this behavior will be discussed in Sect. 4.4.

## 4 Discussions

### 4.1 Arc dynamics characteristics

As expected, the increase in cold wire feed causes an increase in current when the welding power source operates in CV mode. In this mode, the current is linked to wire feed speed (melting wire rate) and varies so that the voltage set-point remains constant. However, this increase in current is not directly linked to an increase in penetration or dilution.

Regarding the stability of the DCW-GMAW process, the introduction of two cold wires leads to a more stable metal transfer in which the instantaneous average voltage is close to the set-point even when high fractions of cold wire are introduced. This seems likely to be related to the stabilization of cathode spots as already reported by Xiang et al. [21] for cold wire TWIN-GMAW.

The metal transfer, measured as the cold wire fraction increases, is governed by the electromagnetic force (Lorentz force) which is proportional to the square of current Eq. 5:

$$F_L = \frac{\mu_0}{4\pi} I^2 f(\theta) \tag{5}$$

where  $F_L$  is the Lorentz force,  $\mu_0$  is the magnetic permeability,  $I$  is the current, and  $f(\theta)$  is the Lorentz force coefficient. Further detail on this relation and the Lorentz force itself can be found in [26]. The results suggest that the increase in current leads to a decrease of the molten droplets since the Lorentz force increases with current.

### 4.2 Peclet ( $Pe$ ) and weld pool convection mechanism

The introduction of cold wire feed causes a widening of the melting pool. This widening is reflected on the energy balance of the melt pool affecting its Peclet number ( $Pe$ ). The Peclet number represents the ratio between convection energy transport and conduction energy transport according to Weckman and Moulton [27]. The  $Pe$  number can be written as Eq. 6:

$$Pe = \frac{vL}{\alpha} \tag{6}$$

where  $v$  is the welding speed,  $L$  is the characteristic length (length) of the melting pool, and  $\alpha$  is the thermal diffusivity. An increase in width will increase the  $Pe$  number meaning the

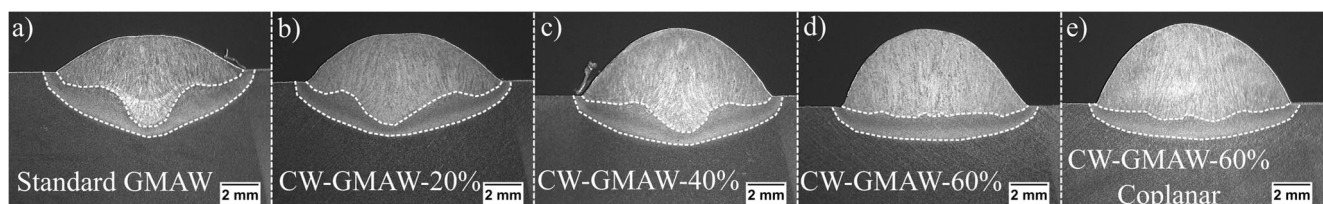
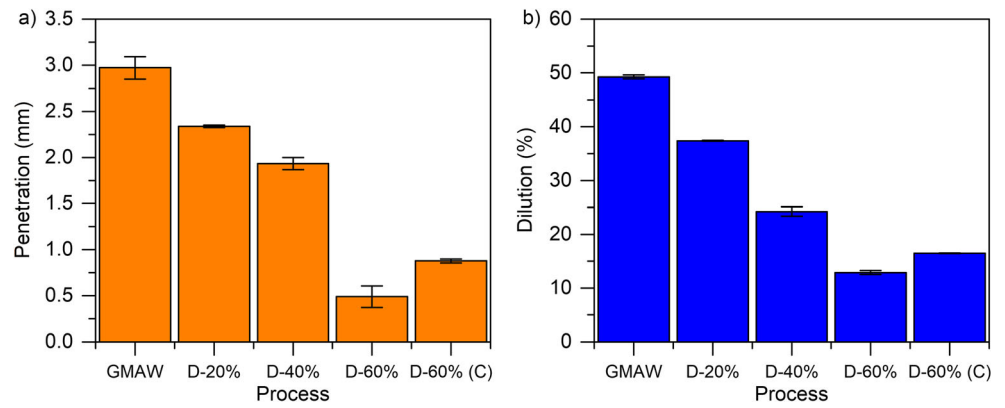


**Fig. 8** Macrographs for the welding conditions: **a** standard GMAW, **b** DCW-GMAW-20%, **c** DCW-GMAW-40%, **d** DCW-GMAW-60%, **e** DCW-GMAW-60%-coplanar

**Fig. 9** Geometric features: **a** penetration, **b** dilution. The (C) stands for coplanar



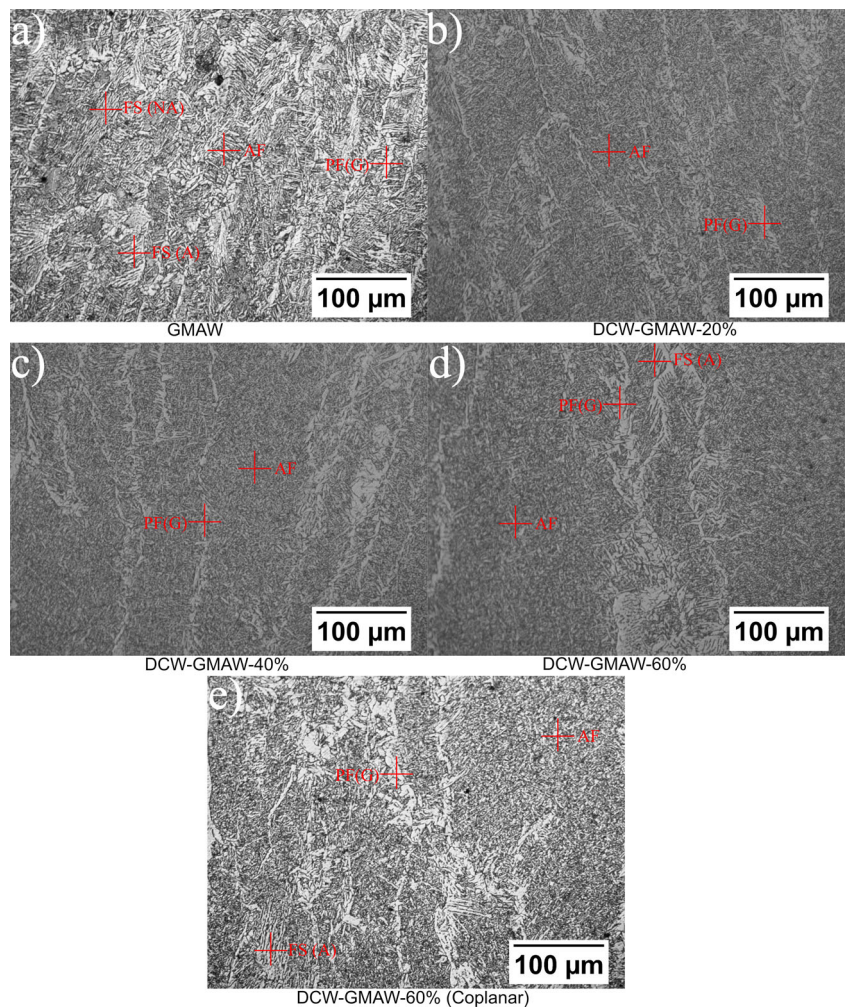
advective transport of heat is more important than the conductive. This change in heat transfer mode importance can induce changes in the cooling rate in the melt pool. In the case of plain carbon steel, the density ( $\rho$ ) equals to  $7.8 \times 10^3 \text{ kg/m}^3$ , the specific heat at constant pressure ( $c_p$ ) equals to  $8 \times 10^2 \text{ J/kgK}$ , and the thermal conductivity ( $k$ ) equals to  $46 \text{ J/smK}$ . One can write the  $Pe$  number as a function of the travel speed

( $v$ ) and the characteristic length ( $L$ ), since  $\alpha = \frac{k}{\rho c_p}$  as can be seen in Eq. 7:

$$Pe = 1.36 \times 10^5 \times v \times L \tag{7}$$

where  $v$  is in units of  $m/s$  and  $L$  is in units of  $m$ . Lancaster [28] pointed out that  $Pe$  higher or equal to 10 indicates that the

**Fig. 10** Micrographs taken at the center of the beads: **a** standard GMAW, **b** DCW-GMAW-20%, **c** DCW-GMAW-40%, **d** DCW-GMAW-60%, **e** DCW-GMAW-60%-coplanar



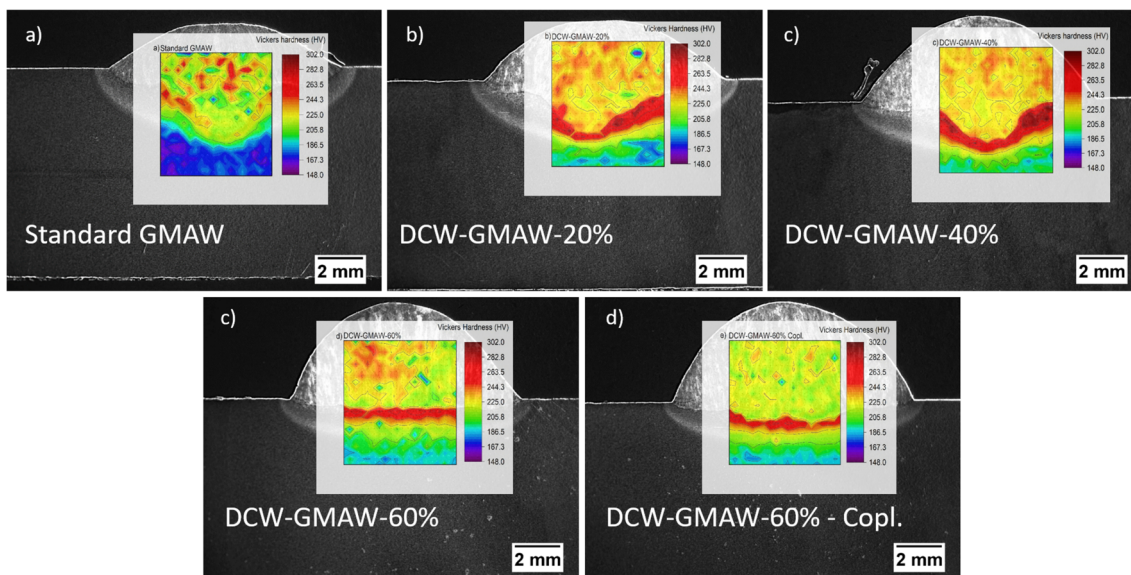


**Fig. 11** Hardness maps of the DCW welds. **a** standard GMAW, **b** DCW-GMAW-20%, **c** DCW-GMAW-40%, **d** DCW-GMAW-60%, and **e** DCW-GMAW-60%-coplanar

convective transfer dominates the heat transfer mechanism. Figure 11 presents the *Pe* numbers for all conditions in this work.

One can see that the introduction of cold wire increases the *Pe* values in the DCW-GMAW conditions regarding the standard GMAW, accounting for an increase in convection as dominant heat transfer mode. This can be attributed to the local feeding of cold wire in one zone of the welding pool, possibly increasing the thermal gradient and ultimately increasing the convection currents. In addition, it seems that this effect is pronounced only for cold wire feeds higher than 40%, which makes sense since the 20% cold metal is fed only in the weld pool edge, possibly with reduced influence on convective current.

Moreover, one can see that when the cold wires are fed coplanarly, the *Pe* value is within the variance of the standard GMAW. Possibly when the cold wires are injected in both sides of the weld pool, there is local reduction of temperatures at both sides causing an overall change in temperature gradient which could change the convective currents more stably, promoting stabilization of the wandering cathode spots, which accounts for the better stability shown in the oscillograms. The reader should refer to Fig. 2e which asserts coefficient of variation smaller than in standard GMAW.

#### 4.2.1 Proposed physical model—Marangoni convection

In order to understand the effect of the double cold wire feed on the convection of the weld pool, it is convenient to write the intensity of the convective currents as a dimensionless number; this is called the Marangoni (*Ma*) number, which can be written according to Mills et al. [29] as:

$$Ma = \frac{d\gamma}{dT} \frac{dT}{dx} \frac{L^2}{\eta\alpha} \tag{8}$$

where  $\frac{d\gamma}{dT}$  is the variation of the weld pool surface tension with the temperature,  $\frac{dT}{dx}$  is the weld pool temperature variation in the direction *x*, *L* is the characteristic length,  $\eta$  is the weld pool molten metal viscosity, and  $\alpha$  is the weld pool molten metal thermal diffusivity.

Taking the *x* direction as the direction parallel to the welding speed direction and admitting that no variation in  $\gamma$  occurs since no tenso-active elements are introduced in the weld pool, the variation of the *Ma* number will depend mainly on the temperature variation.

As reported in a prior work by Xiang et al. [21], the introduction of a cold wire perpendicular to the *x* direction decreased the convective currents accounting the decrease in the cathode spot wandering which causes an improvement in process stability. For the case of DCW-GMAW, when the cold wires are introduced in different planes, the area of the weld pool into which the wires are introduced likely has its temperature reduced by the action of the cold mass that acts as a heat sink. This situation is likely to increase the temperature gradient, consequently increasing the *Ma* number and in the intensity of the convective currents inside the melt pool. Up to the limit, as the cold wire fraction increases, the temperature gradient increases causing an increase in the convective currents until the convective currents inside the melt pool are high enough to disturb the emitting of the cathode spots.

However, it was demonstrated in this work that not only how many cold wires are introduced into the weld pool matters but also how the cold wires are introduced. In fact, when the same 60% cold feed was introduced coplanarly, one can

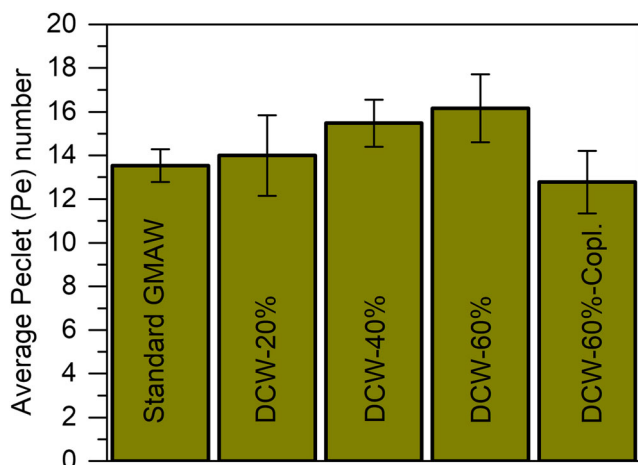


**Fig. 12** Variation of the  $Pe$  numbers for all the conditions. Average of four cross sections

note that the stability increased as can be seen in the area of the corresponding cyclogramme (Fig. 3e). Likely the reason behind is due to the balance in the temperature gradient when the cold wire is introduced at the front and rear of the arc, which reduces the Ma number and the convective currents and accounts for the reduction of the cathode spots wavering on the pool surface.

### 4.3 Dilution, penetration, and microstructures

The relationship between dilution and penetration in standard GMAW is direct. This means that higher penetration leads to higher dilution. As penetration can be modeled by heat and mechanical effect of the droplets [30], either a highly accelerated or hotter droplet will increase penetration. However, in DCW-GMAW, the arc pinned to the cold wires shields the melt pool from droplet impinging momentum. Consider that, the cold wires also act as a thermal barrier when the droplet impinges on it, absorbing heat so that it can be melted while reducing penetration. This explains why while there is an increase in current, the penetration and dilution decrease.

As pointed out, the introduction of cold wire leads to a change in the melting pool form which did not lead to changes on its overall cooling rate in DCW-GMA welds which can be confirmed by the microstructures found in the center of the beads. The microstructures found in the GMAW specimen are a mix of PF and AF, refer to Fig. 10a. With the introduction of the cold wires, the observed amount of acicular ferrite (Fig. 10b–e) did change compared to GMAW. This microstructure is highly dependent on the quantity of inclusions to nucleate heterogeneously [24]; however, the introduction of two cold wires does not appear to increase the amount of inclusions in the molten metal. This factor associated with the cooling rate can explain the constant amount of acicular ferrite observed.

### 4.4 Vickers hardness

As indicated in Fig. 11, specimens with double cold wire feed present higher hardness than the standard GMAW specimen; as noted in the previous section, this is related to the increase in cooling rate in DCW specimens. As the temperature gradient inside the weld pool increases, the cooling rate increases accordingly. The noticed exception is DCW-GMAW-60%-coplanar; this specimen presents hardness similar to the standard GMAW specimen. The reason behind this phenomenon is likely the balance of the thermal gradient inside the weld pool (Figure 12).

In the case of the DCW-GMAW-60%-coplanar setting, the cold wires are introduced trailing and leading the arc which likely balances the thermal gradient when compared to DCW-GMAW-60%, which accounts for the observed higher hardness in DCW-GMAW-60%. This result seems consistent with the qualitative physical model proposed in Sec. 4.2.1 since the thermal gradient in DCW-GMAW-60%-coplanar is likely to be less steep than in the standard DCW-GMAW-60% setting, and so, the strength of the convection currents in the weld pool is lower in DCW-GMAW-60%-coplanar than in the standard DCW-GMAW-60% setting. This explains the better stability in DCW-GMAW-60%-coplanar as indicated in Fig. 3e.

## 5 Conclusions

Bead on plate welds were performed using GMAW and DCW-GMAW to study the process features, stability, and bead morphology and microstructures in DCW-GMAW. The analysis of the results induces the following conclusions:

1. The feasibility of the DCW-GMAW process is demonstrated by the weld bead morphology. No undercuts, humps, or external porosity were found in the beads produced.
2. The introduction of two cold wires seems to stabilize the arc based on narrower scatter of data in the oscillograms as can be seen through the coefficients of variation calculated from the voltage signals where DCW-60% presents an improved stability based on the decrease of 25% in the coefficient of variation in comparison to standard GMAW.
3. The introduction of cold wires increases progressively the hardness of the weld metals. In comparison with standard GMAW, DCW-60% promotes a hardness increase of 10%. However, DCW-60% (coplanar) presents a decrease in hardness of 15% compared to standard GMAW, likely due to changes in heat distribution and cooling rate.

## References

- McPherson NA (2010) Welding issues for ship structures. *J Mar Eng Technol* 9:31–41. <https://doi.org/10.1080/20464177.2010.11020238>
- Mohandas T, Reddy GM, Kumar BS (1999) Heat-affected zone softening in high-strength low alloy steels. *J Mater Process Technol* 88:284–294. [https://doi.org/10.1016/S0924-0136\(98\)00404-X](https://doi.org/10.1016/S0924-0136(98)00404-X)
- Zhang J, Leng J, Wang C (2019) Tuning weld metal mechanical responses via welding flux optimization of TiO<sub>2</sub> content: application into EH<sub>36</sub> shipbuilding steel. *Metall Mater Trans B Process Metall Mater Process Sci* 50:2083–2087. <https://doi.org/10.1007/s11663-019-01645-6>
- Babu SS (2004) The mechanism of acicular ferrite in weld deposits. *Curr Opin Solid State Mater Sci* 8:267–278. <https://doi.org/10.1016/j.cossms.2004.10.001>
- Barbosa LHS, Modenesi PJ, Godefroid LB, Arias AR (2019) Fatigue crack growth rates on the weld metal of high heat input submerged arc welding. *Int J Fatigue* 119:43–51. <https://doi.org/10.1016/j.ijfatigue.2018.09.020>
- Larkin N, Pan ZX, van Duin S et al (2011) Tandem gas metal arc welding for low distortion butt welds. *Adv Mater Res* 337:511–516. <https://doi.org/10.4028/www.scientific.net/AMR.337.511>
- Turichin G, Kuznetsov M, Tsubulskiy I, Firsova A (2017) Hybrid laser-arc welding of the high-strength shipbuilding steels: equipment and technology. *Phys Procedia* 89:156–163. <https://doi.org/10.1016/j.phpro.2017.08.005>
- Näsström J, Brueckner F, Kaplan AFH (2020) A near-vertical approach to laser narrow gap multi-layer welding. *Opt Laser Technol* 121:105798. <https://doi.org/10.1016/j.optlastec.2019.105798>
- Ribeiro RA, dos Santos EBF, Assunção PDC et al (2015) Predicting weld bead geometry in the novel CW-GMAW process. *Weld J* 94:301s–311s
- Assunção PDC, Ribeiro RA, dos Santos EBF et al (2017) Feasibility of narrow gap welding using the cold-wire gas metal arc welding (CW-GMAW) process. *Weld World* 61:659–666. <https://doi.org/10.1007/s40194-017-0466-5>
- Malin VY (1983) The state-of-the-art of narrow gap welding—part I. *Wekding J* 62:22–30
- Malin VY (1983) The state-of-the-art of narrow gap welding—part II. *Wekding J* 62:37–46
- Cabral TS, Braga EM, Mendonça EAM, Scott A (2015) Influence of procedures and transfer modes in MAG welding in the reduction of deformations on marine structure panels. *Weld Int* 29:928–936. <https://doi.org/10.1080/09507116.2014.932993>
- Marques LFN, dos Santos EBF, Gerlich AP, Braga EM (2017) Fatigue life assessment of weld joints manufactured by GMAW and CW-GMAW processes. *Sci Technol Weld Join* 22:87–96. <https://doi.org/10.1080/13621718.2016.1194735>
- Costa ES, Assunção PDC, Dos Santos EBF et al (2017) Residual stresses in cold-wire gas metal arc welding. *Sci Technol Weld Join* 22:706–713. <https://doi.org/10.1080/13621718.2017.1306014>
- Braga EM and Assunção PDC (2013) Welding process gas metal arc welding-double cold wire (GMAW-DCW) 4
- Joseph A, Harwig D, Farson DF, Richardson R (2003) Measurement and calculation of arc power and heat transfer efficiency in pulsed gas metal arc welding. *Sci Technol Weld Join* 8:400–406. <https://doi.org/10.1179/136217103225005642>
- AWS (2005) Specification for carbon steel electrodes and rods for gas shielded arc welding. American Welding Society (AWS), Miami, FL
- (2018) AISI 1020 Steel hot rolled
- Dolby RE (1986) Guidelines for the classification of ferritic steel weld metal microstructural constituents using the light microscope. *Weld World* 24:144–148
- Xiang T, Li H, Wei HL, Gao Y (2016) Effects of filling status of cold wire on the welding process stability in twin-arc integrated cold wire hybrid welding. *Int J Adv Manuf Technol* 83:1583–1593. <https://doi.org/10.1007/s00170-015-7686-x>
- Jorge VL, Gohrs R, Scotti A (2017) Active power measurement in arc welding and its role in heat transfer to the plate. *Weld World* 61:847–856. <https://doi.org/10.1007/s40194-017-0470-9>
- Ribeiro RA, Dos Santos EBF, Assunção PDC et al (2019) Cold wire gas metal arc welding: droplet transfer and geometry. *Weld J* 98:135S–149S. <https://doi.org/10.29391/2019.98.011>
- Abson DJ (2018) Acicular ferrite and bainite in C–Mn and low-alloy steel arc weld metals. *Sci Technol Weld Join* 23:635–648. <https://doi.org/10.1080/13621718.2018.1461992>
- Byun JS, Shim JH, Suh JY et al (2001) Inoculated acicular ferrite microstructure and mechanical properties. *Mater Sci Eng A* 319–321:326–331. [https://doi.org/10.1016/S0921-5093\(00\)02014-1](https://doi.org/10.1016/S0921-5093(00)02014-1)
- Amson JC (1965) Lorentz force in the molten tip of an arc electrode. *Br J Appl Phys* 16:1169–1179. <https://doi.org/10.1088/0508-3443/16/8/316>
- Weckman DC, Moulton JA (2017) Improved formability of fusion welded AA5182-O aluminum tailor welded blanks. *Welding J* 96:319s–333s
- Lancaster JF (1986) *The physics of welding*, 2nd edn. Pergamon Press, Oxford
- Mills KC, Keene BJ, Brooks RF, Shirali A (1998) Marangoni effects in welding. *Philos Trans R Soc A Math Phys Eng Sci* 356:911–925. <https://doi.org/10.1098/rsta.1998.0196>
- Murray PE, Scotti A (1999) Depth of penetration in gas metal arc welding. *Sci Technol Weld Join* 4:112–117. <https://doi.org/10.1179/136217199101537644>

**Publisher's note** Springer Nature remains neutral with regard to jurisdictional claims in published maps and institutional affiliations.